sustainability

MDPI

Article

Exploring a Novel *Aspergillus terreus* Mycelial-Silica Oxide Composite as a Sustainable Adsorbent of Dye Wastewater: Synthesis, Optimization, and Safety Evaluation

Ghada Abd-Elmonsef Mahmoud *, Rania Mahmoud Fouad and Ahmed Y. Abdel-Mallek

Botany and Microbiology Department, Faculty of Science, Assiut University, Assiut 71516, Egypt
* Correspondence: ghadamoukabel@aun.edu.eg

Abstract

Azo dyes demonstrate dose-dependent carcinogenic and mutagenic effects in exposed cells. Among remediation approaches, microbial adsorption is the most sustainable and environmentally friendly method for eliminating azo dyes. A novel *Aspergillus terreus* silica composite was developed as a sustainable adsorbent for crystal violet dye (CVD) removal. The fungal strain was isolated from dye wastewater and was genetically identified by 18S rRNA gene sequencing. Dried mycelia of *A. terreus* (PX920301) were combined with SiO_2 (1:1 *w*/*w*) through iterative hydration-drying cycles, yielding a composite characterized by FTIR analyses. Removal CVD %, adsorption capacity, and CVD residual were calculated, and the adsorption process was optimized using Box–Behnken design (four factors, 25 runs). The biosafety of the composite was assessed for phytotoxicity and microbial toxicity. The composite was also applied to real dyes wastewater collected from the bacteriological laboratory. *Aspergillus terreus*-silica composite showed the highest CVD removal percentage by 85.4%, adsorption capacity (qe) 121.1 mg/L, and lowest CVD residual by 7.26 mg/L, followed by the dried active mycelia (DA-mycelia) with CVD removal 40.23%, adsorption capacity (qe) 57.05 mg/L, and CVD residual by 29.73 mg/L. Optimization data cleared that the maximum experimental values of CVD removal (%) was 99.59% (predicted value 100%) obtained in run number (4) using initial CVD concentration (200 mg/L), pH (8), adsorbent composite weight (0.1 g), and contact time (48 h). Biosafety evaluation demonstrated negligible phytotoxicity against *Triticum aestivum* seedlings post-treatment, with restored germination and growth comparable to controls. Microbial toxicity assays via well-diffusion to seven microbial isolates confirmed no toxic activities against the tested bacteria, yeast, and fungi, underscoring the composite's environmental safety. The composite could decolorize the real dye wastewater of laboratories by 95.37%. In conclusion, *A. terreus* mycelial-silica composite offers a cost-effective, sustainable, and eco-friendly alternative solution for dye bioremediation.

Keywords: bioremediation; industrial dyes; wastewater; fungal mycelia; adsorption; azo dyes

Check for updates

Academic Editors: Mirko Frappa and Francesca Macedonio

Received: 26 March 2026
Revised: 16 April 2026
Accepted: 23 April 2026
Published: 25 April 2026

Copyright: © 2026 by the authors. Licensee MDPI, Basel, Switzerland. This article is an open access article distributed under the terms and conditions of the Creative Commons Attribution (CC BY) license.

1. Introduction

The intrinsic equilibrium of natural ecosystems has been profoundly disrupted by a range of anthropogenic interventions [1]. The generation and subsequent accumulation of diverse industrial pollutants during processing, particularly within the textile, leather, and printing sectors, lead to the discharge of highly contaminated dye wastewater streams [2].

The discharge of colored wastewater from industries into aquatic ecosystems reduces light penetration and lowers the photosynthesis rates of algae and aquatic plants [3]. The high chemical and biological oxygen demand generated from toxic dyes depletes the dissolved oxygen, causing fish kills and loss of biodiversity in rivers and streams [4,5]. Moreover, under anaerobic conditions, dyes in wastewater can undergo biotransformation to yield aromatic amines with toxic, mutagenic, and carcinogenic properties [6].

Azo dyes represent the largest and most extensively used class of industrial synthetic colorants, covering 60–70% of the global dye production [7], characterized by their azo linkages (–N=N–), which confer high stability [8]. From azo dyes, CVD is a cationic triphenylmethane azo dye extensively used in textile dyeing, paper printing, leather processing, and as a biological stain in bacteriological and medical laboratories [9,10]. Its widespread utilization has led to significant environmental dissemination, primarily through the discharge of untreated CVD or inadequately treated industrial CVD that effluents into aquatic ecosystems [11]. Their presence in water bodies could induce oxidative stress, cytotoxicity, and damage to vital organs of exposed organisms [11–13]. Moreover, CVD has been reported to exhibit mutagenic and potentially carcinogenic properties, raising serious concerns regarding its impact on both environmental and human health [10,14]. The persistence, bioaccumulation potential, and hazardous biological effects underscore the urgent need for effective and sustainable remediation strategies to mitigate CVD environmental spread. Although various combinations of physical and chemical CVD decolorization methods were applied, biological remediation represents the best eco-friendly, cost-effective and sustainable way [15]. From the biological methods, the adsorption technique has received considerable attention for its flexibility and ease of use without the need for highly complex equipment [16].

Fungal mycelia represent a natural, low-cost, and renewable polymer material composed of glucan, chitin, and proteins [17]. Fungal biomass in dead form could be used effectively as an adsorbent agent for their unique structure and bio-adhesive properties [18]. These adsorption properties have recently received superior attention as environmentally friendly, economical, operational flexibility, and low-cost, efficient alternative for pollutants remediation from wastewater [15,19]. Mycelium-based composite is a term used to describe any new adsorbent material that is established by the combination of fungal mycelia and other materials through bio-fabrication processes [20,21]. This biological composite could be used for environmental repair, pollutant removal, packaging, building materials, and even in wearable materials [15,22,23]. Fungal mycelium-based bio-composites offer sustainable options for treating real wastewater by effective adsorption of heavy metals, dyes, and organic pollutants [21,23].

Silicon dioxide (SiO_2, silica) plays a pivotal role in pollutant removal due to its unique physicochemical properties by possessing a high surface area, porous structure, and surface silanol (–Si–OH) groups, which present various active sites for the adsorption process of contaminants [24]. These silanol groups enable strong interactions with pollutants through mechanisms such as hydrogen bonding, electrostatic attraction, and surface complexation, making silica particularly effective in removing dyes, heavy metals, and organic compounds from aqueous systems [25,26]. Additionally, it has a chemically stable functionalized structure, is non-toxic, and cost-effective, which could be functionalized to enhance its adsorption efficiency [27]. The compatibility of hybrid composites with biological materials, such as silica–microbial systems, supports the combination of high adsorption capacity with eco-friendly characteristics.

The present study aimed to develop and evaluate a novel, eco-friendly *Aspergillus terreus*–silica composite as an efficient biosorbent for the CVD removal from aqueous solutions. First, the study aims to isolate a potent azo dye biosorbent from industrial dye wastewater. In-

vestigate the adsorption performance of the dried fungal mycelia and the composite by determining the removal efficiency, adsorption capacity, and residual dye concentration, as well as to optimize the adsorption process using Box–Behnken experimental design. Furthermore, the study intended to assess the environmental biosafety of the developed composite through phytotoxicity and microbial toxicity assays, and to validate its practical applicability in treating real dye-contaminated wastewater.

2. Materials and Methods

2.1. Isolation of Fungal Adsorbent

Fungal adsorbent was isolated from the dye wastewater of laundry in Assiut, Egypt. The dye wastewater was analyzed for its physiochemical characteristics, including pH, electrical conductivity, total dissolved solids and dissolved oxygen using a Jenway Model 3450 conductivity/pH meter (Jenway Company, Essex, UK). For fungal isolation, modified mineral salt medium (MSM) was prepared and consisted of (g/L): 10.0 NaCl, 10.0 glucose, 1.0 KH_2PO_4, 0.2 $(NH_4)_2SO_4$, 0.05 $CaCl_2$, 0.05 $MgSO_4$, 18.0 agar and 1.0 methylene blue dye (as an indicator for the fungal decolorization efficiencies) with an initial pH of 6 [28]. One ml of the dye wastewater was transferred into a sterilized Petri dish and mixed with 25 mL of sterilized MSM medium. After solidification, the plates were incubated at 30 ± 1 °C for one week. Generated fungal colonies that decolorized the methylene blue color were selected and purified on MSM plates. The isolated fungal species was identified primarily based on the macroscopic and microscopic features following the keys and descriptions of Raper and Fennell [29] for *Aspergillus* species and Moubasher [30] for fungi using Czapek's dextrose agar medium (1% dextrose, 0.1% KH_2PO_4, 0.3% $NaNO_3$, 0.05% $MgSO_4$, 0.001% $FeSO_4$, and 1.8% agar) after 5 days of incubation at 30 ± 1 °C.

2.2. Molecular Identification of Fungal Adsorbent

The *Aspergillus* isolate was re-cultured on a sterile Czapek's dextrose agar plate and incubated at 30 ± 1 °C for 5 days. Then, small parts of *Aspergillus* mycelium were scraped and transferred to 100 µL of sterile distilled water, boiled for 15 min at 100 °C and stored at −80 °C. Dead *Aspergillus* cells were sent to SolGent Company (Daejeon, Republic of Korea) for DNA extraction and sequencing. *Aspergillus* DNA was extracted using the Solg™ Genomic DNA Prep Kit. Internal transcribed spacer region (ITS) was amplified using universal primers: ITS1 (5′-TCC GTA GGT GAA CCT GCG G-3′), and ITS4 (5′-TCC TCC GCT TAT TGA TAT GC-3′). The process of amplification was done by ABI, 9700 thermal cycler using the polymerase chain reaction (PCR) mixtures: 10 mM dNTP (T) 0.5 µL, 10× EF-Taq buffer 2.5 µL, primer (F-10p) and (R-10p) 1.0 µL for each, template 1.0 µL, EF-Taq (2.5U) 0.25 µL, DW to 25 µL. One round of denaturation for 15 min at 95 °C followed by 30 denaturation cycles at 95 °C for 20 s, then annealing for 40 s at 50 °C and extension for 1 min at 72 °C [31,32]. The purified PCR products were sequenced, and the data were analyzed using BLAST from the National Center of Biotechnology Information (NCBI) website. Sequences obtained together with those retrieved from the GenBank database (http://www.ncbi.nlm.nih.gov) (accessed on 13 January 2026) were subjected to the Clustal W analysis using MegAlign software version 5.05 (DNASTAR Inc., Madison, WI, USA) for the phylogenetic analysis [33].

2.3. Detecting the CVD Maximum Absorbance and Preparing Its Standard Curve

Before starting the experiments, we scanned the dye over a range of wavelengths (nm) to find the maximum absorbance (λmax) of the CVD ($C_{25}H_{30}ClN_3$). Ultraviolet visible spectroscopic analysis (UV/Vis) was utilized to measure the maximum absorbance of the CVD solution with a concentration of 50 mg/L using Thermo Evolution 300, UV-VIS

Spectrophotometer Model EVO300 PC, USA with a range of 190−1100. To calculate the residual CVD concentrations, a standard curve of the CVD water solution was prepared and was conducted with a range of 0–100 mg/L using a spectrophotometer at the maximum absorbance (582 nm).

2.4. Preparation of Fungal Mycelia and Testing Their Adsorption Efficiencies

For mycelia preparation, a spore suspension of *A. terreus* (PX920301) with 10^8 spores/mL was inoculated into 200 mL potato dextrose broth medium and incubated with shaking at 30 ± 1 °C with 150 rpm/min for 72 h. After the incubation period, the mycelia were collected using filtration on Whitman filter paper and washed three times with sterilized distilled water to remove any spores. The mycelia were separated into two parts. The first part was autoclaved at 121 °C for 20 min to inactivate the fungal cells and then dried using a hot air oven at 70 °C overnight to form inactive dried mycelia (ID-mycelia). The second part was directly dried in a hot air oven at 70 °C overnight as active dried mycelia (AD-mycelia). Both types of mycelia were tested for their CVD adsorption efficiencies; Falcon tubes containing 20 mL of 50 mg/L CVD in sterile double-distilled water were prepared. Each tube was inoculated with 0.2 g of ID-mycelia and AD-mycelia, then incubated at 30 ± 1 °C in a shaking incubator (150 rpm/min) for 24 h. Each experiment was conducted with three replicates. The adsorption efficiencies were examined using a spectrophotometer at 582 nm, and the dye removal percentage was calculated following the equation:

$$R\ (\%) = ((C_i - C_e)/C_i) \times 100 \quad (1)$$

$$qe = ((C_i - C_e) \times (V))/M \quad (2)$$

where R (%): CVD removal percentage, C_i: CVD initial absorbance, and C_e: CVD final absorbance after the incubation time; qe (mg/L) is the adsorption capacity of the adsorbents; V is the volume of CVD solution used (L), and M is the amount of adsorbent used (g/L) [34,35].

2.5. Aspergillus terreus-Silica Composite Preparation and Characterization

Mycelia-based composite of *A. terreus* (PX920301) and silica oxide (SiO_2) was prepared as shown in Figure 1. Ten grams of silica oxide were mixed with active dried mycelia (1:1; g), then 100 mL of sterilized distilled water was added, and the mixture was stirred evenly for 15 min with a magnetic stirrer. Then the composite was left to dry in the oven at 70 °C. After drying, the composite was stirred again with another 100 mL of sterilized distilled water for 15 min and dried in the oven at 70 °C; this step was repeated three times with the same procedures. To test its decolorization efficiencies, Falcon tubes containing 20 mL of 50 mg/L CVD were inoculated with a 0.2 g composite and incubated at 30 ± 1 °C in a shaking incubator (150 rpm/min) for 24 h. The experiment was conducted with three replicates, and the adsorption efficiencies were examined using a spectrophotometer at 582 nm. Removal (%), adsorption capacity (qe, mg/L), and CVD residual (mg/L) were calculated. Fourier transform infrared (FTIR) spectroscopy was used to understand the characteristics of the composite and to identify the functional groups with a scanning range of 4000−500 cm^{-1} with a 1 cm^{-1} spectral resolution using a Nicolet iS10 FTIR Spectrometer, USA.

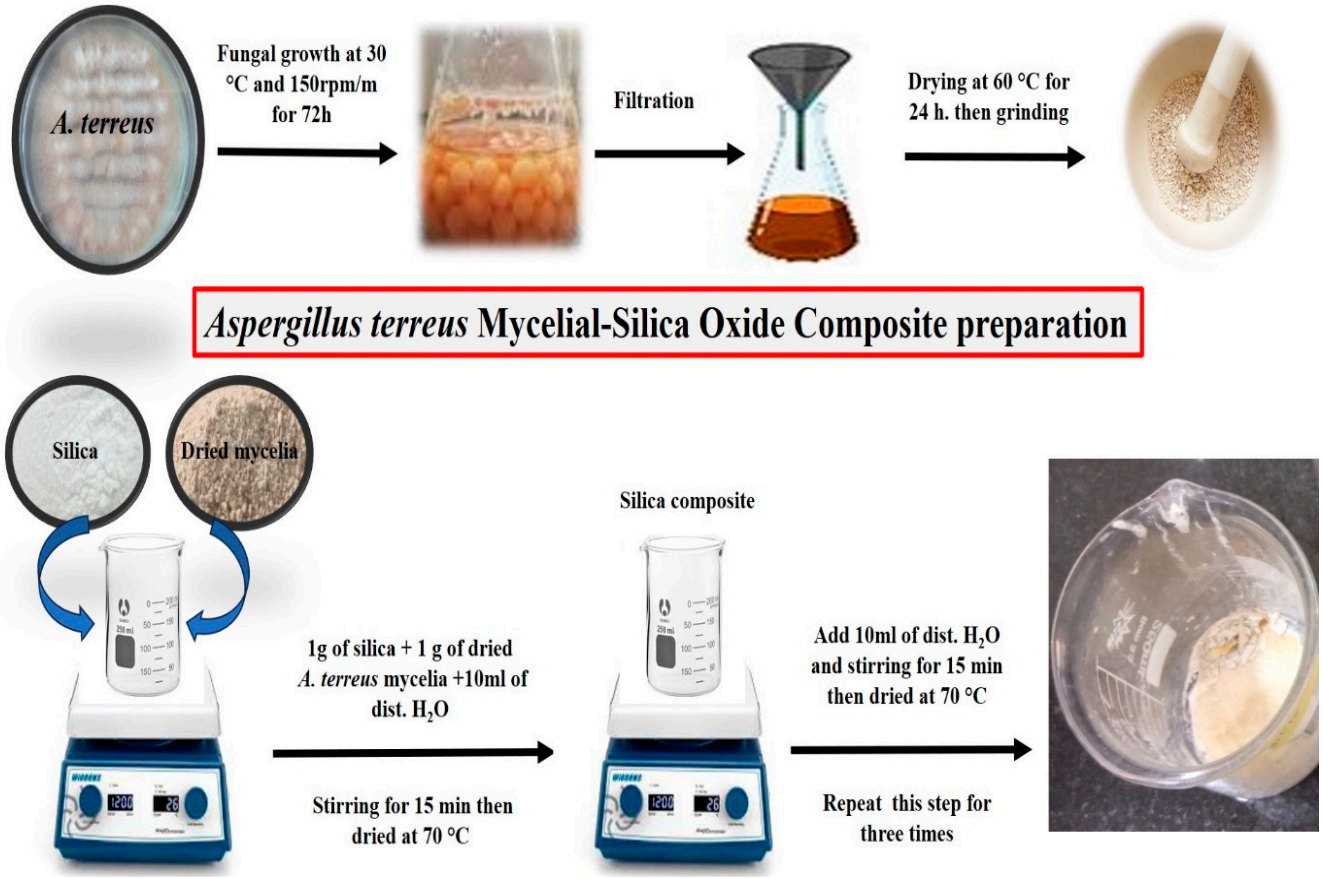


Figure 1. *Aspergillus terreus*-silica composite preparation process.

2.6. Optimizing the CVD Removal Process Using Box–Behnken Experimental Design

A Box–Behnken statistical design (BBD) was employed to optimize the adsorption process of CVD by *A. terreus* silica composite in water solution, while evaluating the main, interaction, and quadratic effects of four independent variables. The three-level, four-factor design comprised 25 experimental runs to model quadratic responses via second-order polynomial equations. Independent variables including initial CVD concentration (50, 100 and 200 mg/L; A), pH (4, 6, and 8; B), adsorbent composite weight (0.05, 0.1, 0.2 g/10 mL; C), and contact time (24, 48, and 72 h.; D) were tested at low (−1), central (0), and high (+1) levels [36], as detailed in Table 1. Nonlinear quadratic models were fitted using Equation (3) as clarified by Liu et al. [37]:

$$Y = \beta_0 + \sum \beta_i x_i + \sum \beta_{ii} x_i^{\,2} + \sum \beta_{ij} x_{ij} \quad (3)$$

where Y represents the predicted CVD removal (%) using *A. terreus*-silica composite; β_0 is the intercept; β_i denotes the linear coefficients; β_{ii} the quadratic coefficients; β_{ij} the interaction coefficients; and x_{ij} the coded levels of the independent variables. Variable interactions were visualized using three-dimensional response surface plots. Model adequacy was assessed via diagnostic plots comparing observed versus predicted values, alongside comprehensive statistical analyses (ANOVA, lack-of-fit tests, and coefficient of determination R^2). Optimal conditions were validated by repeating the experiment three times and applying Derringer's desirability function to confirm model robustness.

Table 1. Box–Behnken design with four variables: initial CVD concentration (mg/L, A), pH (B), adsorbent composite weight (g, C), and contact time (h., D) with actual and/or predicted responses of CVD removal (%) using *A. terreus*-silica composite.

Run Order	Initial CVD Concentration (mg/L, A)	pH (B)	Adsorbent Composite Weight (g, C)	Contact Time (h., D)	Actual Value	Predicted Value
1	−1	−1	0	0	70.41	68.82
2	1	−1	0	0	93.03	93.51
3	−1	1	0	0	71.29	69.59
4	1	1	0	0	99.59	100.00
5	0	0	−1	−1	89.16	90.99
6	0	0	1	−1	91.87	93.82
7	0	0	−1	1	65.42	64.86
8	0	0	1	1	65.49	64.72
9	−1	0	0	−1	65.21	61.33
10	1	0	0	−1	84.50	82.18
11	−1	0	0	1	70.85	72.39
12	1	0	0	1	73.27	71.69
13	0	−1	−1	0	83.11	83.11
14	0	1	−1	0	19.72	21.55
15	0	−1	1	0	35.28	36.58
16	0	1	1	0	93.18	91.36
17	−1	0	−1	0	76.48	74.45
18	1	0	−1	0	87.33	88.26
19	−1	0	1	0	31.34	33.41
20	1	0	1	0	84.21	82.30
21	0	−1	0	−1	96.20	99.91
22	0	1	0	−1	88.87	87.40
23	0	−1	0	1	69.69	72.25
24	0	1	0	1	82.14	81.13
25	0	0	0	0	95.16	96.17

2.7. Biosafety Analysis of A. terreus-Silica Composite

2.7.1. Phytotoxicity Test

Phytotoxicity of CVD wastewater treated with an *A. terreus*-silica composite was assessed using *Triticum aestivum* L. (wheat) grains. Healthy grains were supplemented from the agricultural research center; the grains were surface sterilized by immersion in ethanol (70%) for 3 min, and sodium hypochlorite (NaOCl 1%) for 1 min, followed by three rinses in sterile distilled water. About 75 grains were divided into three groups (n = 3 plate replicates/group, 25 grains/each plate): (A) water control; (B) untreated CVD solution; (C) treated CVD solution post-*A. terreus*-silica composite treatment. Grains were imbibed in respective solutions in a sterile Petri dish for 24 h at 30 ± 1 °C. Subsequently, grains were transferred to other sterilized Petri dishes lined with filter paper, where dishes were maintained moist using the corresponding treatment solutions and incubated at 30 ± 1 °C [38,39]. Seedling growth parameters, including germination percentage (following Equation (4)), plumule length and radical length were measured.

$$\text{Germination (\%)} = (\text{Total number of germinated grains}/\text{Total number of grains}) \times 100 \quad (4)$$

2.7.2. Microbial Toxicity

Toxicity of the treated CVD wastewater with *A. terreus*-silica composite was tested on the microbial growth of Gram-positive bacteria (*Staphylococcus aureus*), Gram-negative bacteria (*Escherichia coli*, *Klebsiella pneumoniae*, and *Pseudomonas aeruginosa*), yeast (*Candida albicans*) and filamentous fungi (*Aspergillus flavus* and *Aspergillus niger*) by measuring the zone of inhibition using the well-diffusion method [36]. Nutrient agar plates (for bacterial tests) and Czapek's dextrose agar plates (for fungal and yeast tests) were prepared and supplemented with 1 mL of inoculum (10^6 CFU/mL) [32]. In each plate, three wells were created using

a sterilized cork borer and supplemented with 50 µL of treated CVD sample, compared with the untreated CVD sample with the same dye initial concentration. The plates were incubated at 30 °C for 48 h (bacteria), 3 days (yeast), and 5 days (filamentous fungi). The developed inhibition zones were measured in all treatments for each microbial strain with three replicates.

2.8. Application of A. terreus-Silica Composite in Real Wastewater

Dyes wastewater with CVD were collected in clean tanks from the bacteriological laboratory, Faculty of Science, Assiut, Egypt. *A. terreus*-silica composite was used as an adsorbent agent under the optimum conditions of CVD removal by Box–Behnken statistical design (BBD). The composite effectiveness in adsorption was detected using Ultraviolet visible spectroscopic analysis (UV/Vis) and the decolorization percentage (%) was calculated.

2.9. Statistical Analysis

Data were analyzed using multiple regression within Design-Expert v7.0.0 (Stat-Ease, USA). Quadratic effects and variable interactions were evaluated via one-way ANOVA at a significance level of $p \leq 0.05$.

3. Results

3.1. Isolation and Identification of Fungal Adsorbent

Aspergillus terreus strain AUMC 16983 was isolated from dye-contaminated wastewater with pH 8.3, electrical conductivity (EC) 620 µS, total dissolved solids (TDS) 379 mg/L and dissolved oxygen (DO) 1.87 mg/L. Phenotypic morphology of the fungus based on macroscopic and microscopic features was performed on Czapek's dextrose agar medium, as illustrated in Figure 2A–C. The fungus was characterized by rapidly growing cinnamon-brown colored aerial mycelia (Figure 2A). Microscopically, it has columnar conidial heads (Ch) on hyaline, smooth conidiophores (Cp) carrying vesicle (Vi), biseriate phialides (Ph) and globose to sub-globose conidia (Co) (Figure 2B,C). The phylogenetic tree based on ITS sequences of ribosomal DNA of *A. terreus* strain AUMC 16,983 (PX920301) was arrow-aligned with closely related *Aspergillus* strains accessed from GenBank (Figure 3). This strain showed 97.35–100% identity and 97–100% coverage with several strains of the same species, including the type material *A. terreus* strain ATCC 1012 (Accession NR_131276). *Penicillium chrysogenum* is included as an outgroup strain (Figure 3).

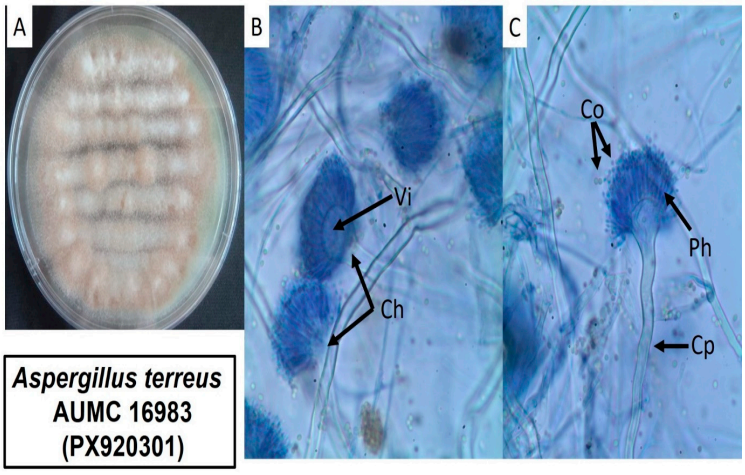


Figure 2. *Aspergillus terreus* strain AUMC 16983 (PX920301) grows on Czapek's dextrose agar medium, clearing the fungus aerial mycelia (**A**), conidial head (Ch), Conidiophore (Cp), Vesicle (Vi), Phialid (Ph), and Conidia (Co), as shown in (**B**,**C**) figures, scale bar, 10 µm.

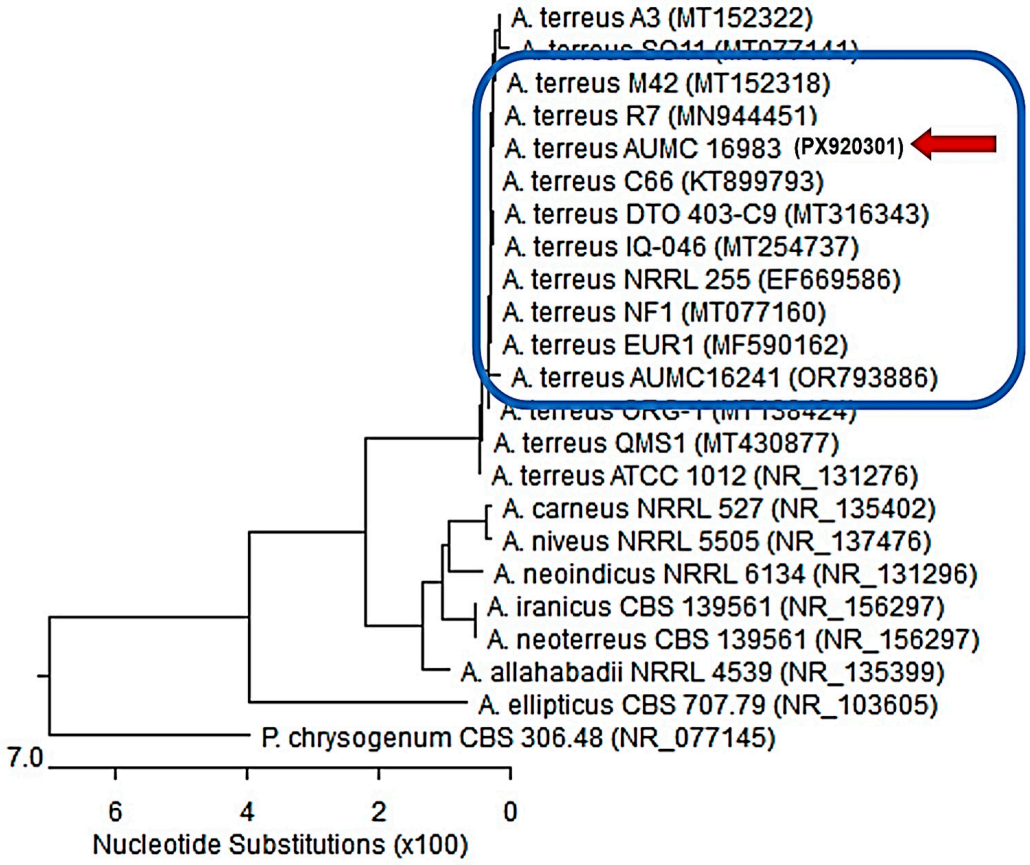


Figure 3. Phylogenetic tree based on ITS sequences of rDNA of the fungal strain isolated in the present study (*Aspergillus terreus* strain AUMC 16983 (PX920301), arrowed), aligned with closely related strains accessed from the GenBank. This strain showed 97.35–100% identity and 97–100% coverage with several strains of the same species, including the type material *Aspergillus terreus* strain ATCC 1012 (Accession NR_131276). [A. = *Aspergillus*, P. = *Penicillium*].

3.2. The Adsorption Efficiencies of CVD Using Aspergillus terreus (PX920301) Dried Mycelia and Silica Composite

The ultraviolet-visible absorption (UV/Vis) spectra of the CVD solution are shown in Figure 4A, demonstrating that the maximum absorbance was 1.667 at 582 nm, which is maintained throughout the experiment. Moreover, the standard curve of the CVD utilized in the experiments was performed with the range of 0–100 mg/L (Figure 4B). Removal (%), adsorption capacity (qe, mg/L), and CVD residual (mg/L) at 50 mg/L concentration using *Aspergillus terreus* (PX920301) silica composite, dried active mycelia (DA-mycelia), and dried inactive mycelia (DI-mycelia) with an adsorbent weight of 0.2 g/20 mL dye solution, as clarified in Figure 5. *Aspergillus terreus* (PX920301) silica composite showed the highest CVD removal percentage by 85.4%, adsorption capacity (qe) 121.1 mg/L, and lowest CVD residual by 7.26 mg/L, followed by the dried active mycelia (DA-mycelia) with CVD removal 40.23%, adsorption capacity (qe) 57.05 mg/L and CVD residual by 29.73 mg/L. However, dried inactive mycelia (DI-mycelia) scored CVD removal of 12.9%, adsorption capacity (qe) 18.35 mg/L and CVD residual by 43.31 mg/L. It is clear that dried active mycelia (DA-mycelia) have higher efficiencies of adsorption than DI-mycelia, and are more suitable for the composite preparation (Figure 5).

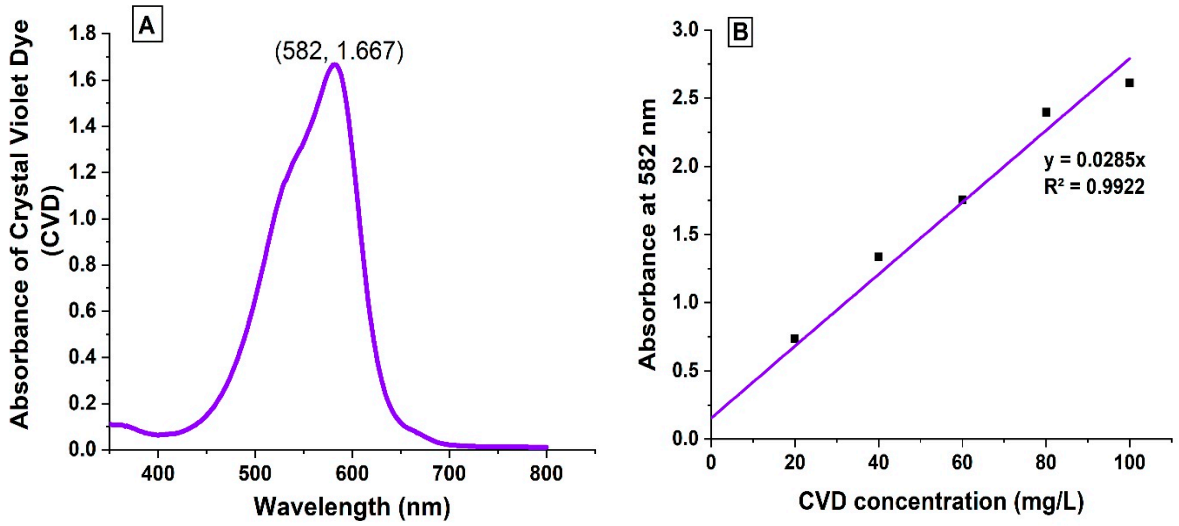


Figure 4. (**A**) Ultraviolet-visible absorption (UV/Vis) spectra of the CVD solution. (**B**) Standard curve of the CVD utilized in the experiments with a range of 0–100 mg/L.

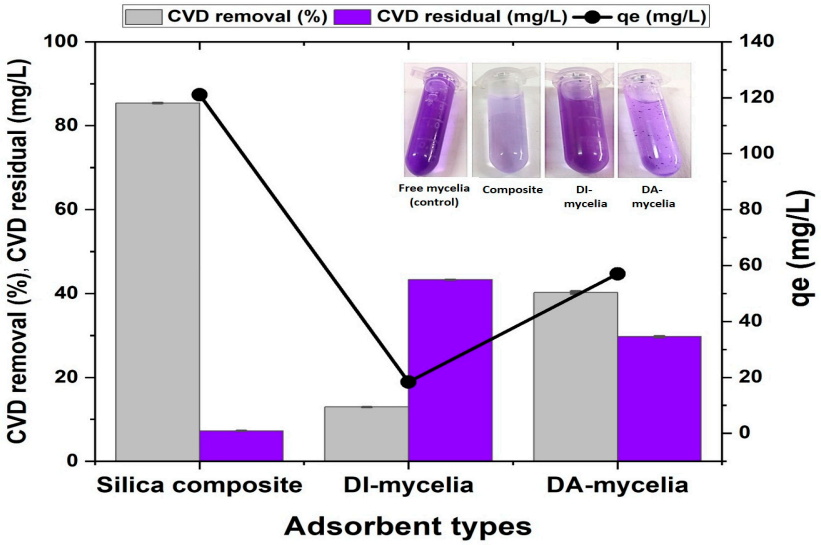


Figure 5. Removal (%), adsorption capacity (qe, mg/L), and CVD residual (mg/L) of CVD at 50 mg/L concentration using *Aspergillus terreus* (PX920301) silica composite, dried active mycelia (DA-mycelia), and dried inactive mycelia (DI-mycelia) with an adsorbent weight of 0.1 g/10 mL dye solution.

3.3. Characterization of the Aspergillus terreus Silica Composite

Aspergillus terreus dried mycelia showed unique FTIR bands including 3416.42 cm^{-1}, 2929.947 cm^{-1}, 2859.555 cm^{-1}, 1628.659 cm^{-1}, 1114.701 cm^{-1}, and 1018.756 cm^{-1}. These bands also appeared in the silica composite FTIR, which confirmed the formation of *A. terreus* mycelia silica composite (Figure 6). Moreover, silica oxide showed sharing bands with *A. terreus* mycelia silica composite, including 1114.701 cm^{-1}, which was inside the region of 1200–1000 cm^{-1}, indicating (Si–O–Si) asymmetric stretching of the silica network (Figure 6). The FTIR spectra of treated CVD with *A. terreus* mycelia silica composite showed the generation of new peaks compared with the FTIR chromatogram of the composite before treating at 2856.104 cm^{-1}, 1749.147 cm^{-1}, 1643.08 cm^{-1}, 1558.226 cm^{-1}, 1459.872 cm^{-1} and 723.1865 cm^{-1}. These peaks confirmed the adsorption of the CVD on the composite (Figure 7).

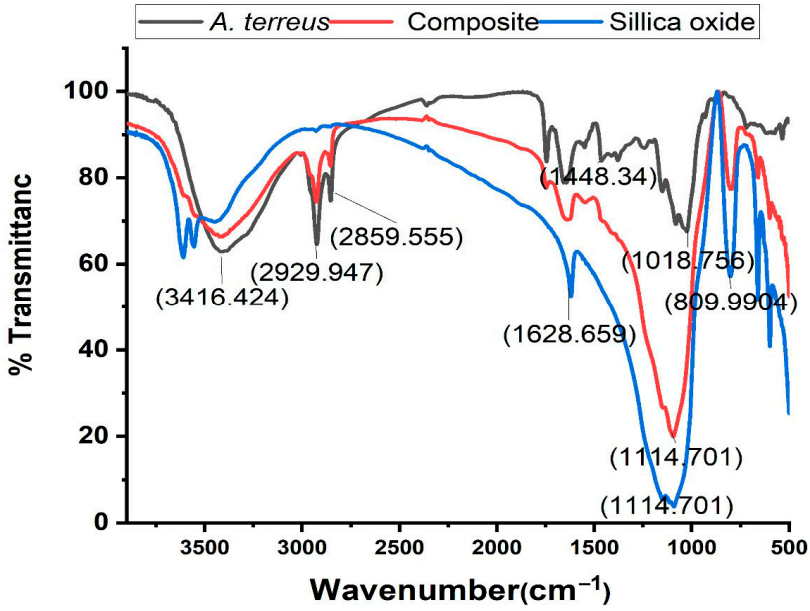


Figure 6. FTIR analysis of *A. terreus*-silica composite compared with the dried *A. terreus* mycelia and silica oxide chromatogram.

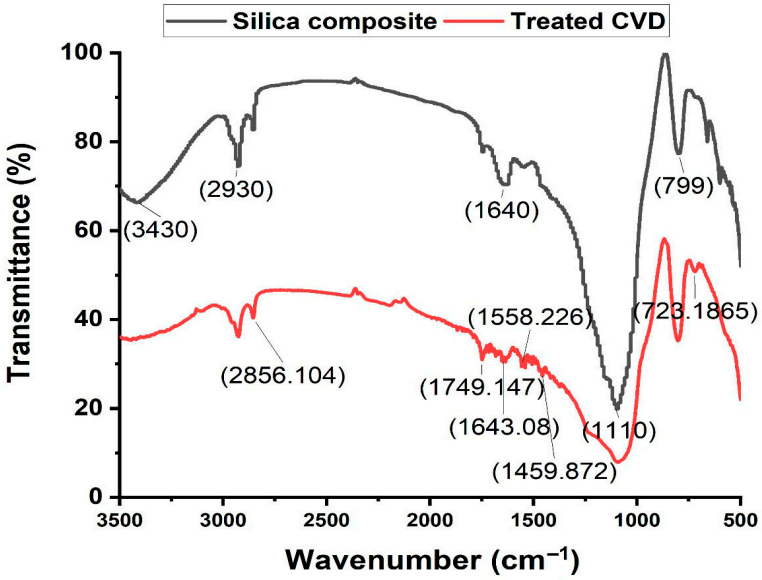


Figure 7. FTIR analysis of *A. terreus*- silica composite before and after treating the CVD wastewater.

3.4. Optimizing the Crystal Violet Adsorption Process Using Box–Behnken Design

In order to study the various factors affecting the adsorption efficiencies of *A. terreus* silica composite, Box–Behnken statistical design (BBD) with multifactorial analysis represents the best choice to study not only the effect of each individual factor but also their interactions. The BBD was employed to optimize the adsorption process of CVD by *A. terreus*-silica composite, evaluating the interactions and quadratic effects of four independent variables. The three-level, four-factor design comprised 25 experimental runs to model quadratic responses via second-order polynomial equations. Independent variables of initial CVD concentration (50, 100 and 200 mg/L; A), pH (4, 6, and 8; B), adsorbent composite weight (0.05, 0.1, 0.2 g; C), and contact time (24, 48, and 72 h.; D) were tested at low (−1), central (0), and high (+1) levels, as detailed in Table 1. The statistical coefficient (R^2) was also determined to evaluate the model accuracy and fitting; R^2 values of CVD removal (%) were 0.9914 and an adjusted R^2 value of 0.9795, which indicated that the variations were

explained effectively by the statistical model. The predicted values of tested runs were scored using Equation (3) for the second-order polynomial; the predicted values of CVD removal (%) were computed using the second-order polynomial Equation (3). The coded equation is useful for identifying the relative impact of the factors by comparing the factor coefficients, the predicted values calculated by Equation (5) as follows:

$$\text{Removal (\%)} = 83.11 + (-16.97)\,A + (+2.32)\,B + (+13.41)\,C + (+12.01)\,D + (+2.86)\,AB + (+16.39)\,AC + (+7.42)\,AD + (+0.270)\,BC + (-2.48)\,BD + (-4.50)\,CD + (-5.74)\,A^2 + (+6.12)\,B^2 + (-9.05)\,C^2 + (-7.57)\,D^2 \quad (5)$$

Maximum experimental value of CVD removal (%) was 99.59%; whereas the corresponding predicted value was 100% obtained in run number (4) using initial CVD concentration (200 mg/L; A), pH (8; B), adsorbent composite weight (0.1 g; C), and contact time (48 h; D); however the lowest CVD removal (%) was 19.72%; whereas the corresponding predicted value was 21.55% obtained in run number (14) using initial CVD concentration (100 mg/L; A), pH (8; B), adsorbent composite weight (0.05 g; C), and contact time (48 h; D). The predicted values of CVD removal (%) were found to be very close to the response model experimental data, indicating that the established model is accurate, as shown in Table 1 and Figure 8. Moreover, the statistical model accuracy, suitability, and significance of the quadric polynomial Equation 3 were examined with one-way analysis of variance (ANOVA) as established in Table 2.

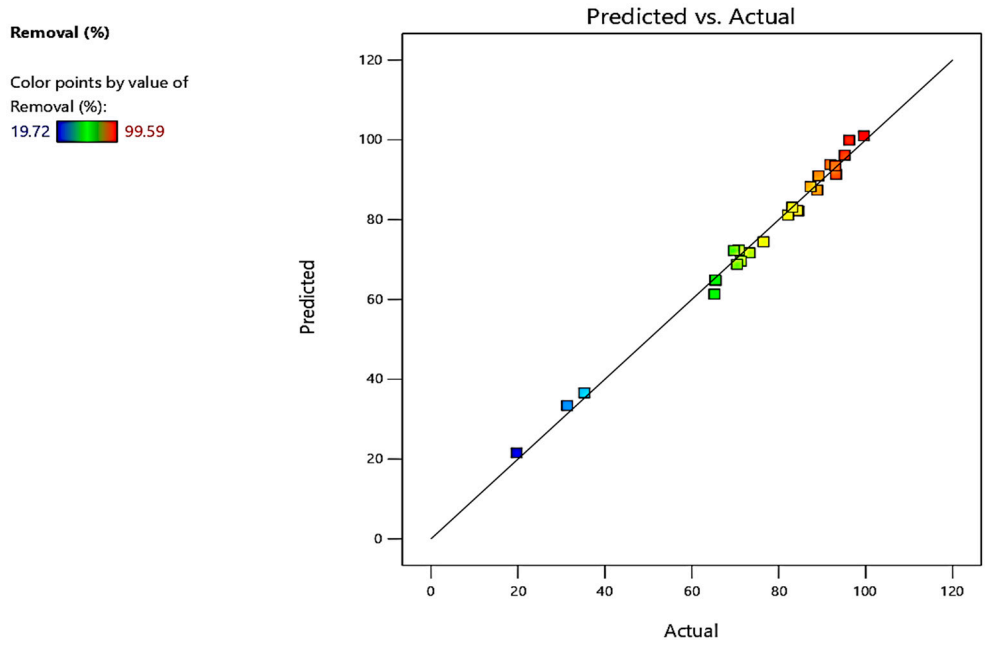


Figure 8. The CVD removal (%) actual and predicted values of the Box–Behnken statistical design.

The Model *F*-value of 82.76 implies the model is fitted, where *p*-values less than 0.05 indicate model terms are significant. In this case, A (initial CVD concentration), B (pH), C (adsorbent composite weight), D (contact time), AC (initial CVD concentration* adsorbent composite weight), AD (initial CVD concentration* contact time), CD (adsorbent composite weight* contact time), A^2, B^2, C^2, D^2 are significant model terms. Values greater than 0.05 indicate the model terms are not significant as in AB (initial CVD concentration* pH), BC (pH* adsorbent composite weight), BD (pH* contact time), and CD (adsorbent composite weight * contact time) (Table 2).

Table 2. ANOVA results for the Box–Behnken quadratic model of the adsorption process (removal %) of CVD by *A. terreus*-silica composite in water solution.

Source	Sum of Squares	df	Mean Square	*F*-Value	*p*-Value
Model	10,051.52	14	717.97	82.76	<0.0001
A-Initial concentration (mg/L)	3455.77	1	3455.77	398.34	<0.0001
B-pH	64.45	1	64.45	7.43	0.0214
C-Composite weight (g)	2156.60	1	2156.60	248.58	<0.0001
D-Contact time (h)	1729.44	1	1729.44	199.35	<0.0001
AB	32.78	1	32.78	3.78	0.0806
AC	1073.87	1	1073.87	123.78	<0.0001
AD	220.08	1	220.08	25.37	0.0005
BC	0.2916	1	0.2916	0.0336	0.8582
BD	24.50	1	24.50	2.82	0.1238
CD	80.91	1	80.91	9.33	0.0122
A^2	93.18	1	93.18	10.74	0.0083
B^2	105.72	1	105.72	12.19	0.0058
C^2	231.42	1	231.42	26.68	0.0004
D^2	161.68	1	161.68	18.64	0.0015

Response surface plots and the interaction plots are drawn for the 3D visualization of the cleared interaction between pairs of the two factors when the other factor is constant, as shown in Figure 9, representing significant effects of the CVD removal (%) using *A. terreus*-silica composite. The preceding results indicated the impacts of four variables on CVD removal (%) over 25 separated runs: initial CVD concentration (mg/L, A), pH (B), adsorbent composite weight (g, C), and contact time (h, D); nevertheless, the most desired concentrations of the variables must be calculated from the three tested values. Derringer's desirability function was used to calculate an optimal variable concentration for high CVD removal (%). By applying the function, the obtained optimum levels were initial CVD concentration (200 mg/L; A), pH (8; B), adsorbent composite weight (0.1 g/10 mL; C), and contact time (48 h; D), which were the best levels and gave desirability equal to 1.000 for CVD removal (%) as shown in Figure 10. In addition, three repeated trials of the optimum parameters were conducted for model validation, where actual values matched the projected values once the desirability functions were set, demonstrating the sufficiency of the quadratic model devised for enhancing CVD removal (%).

3.5. Phytotoxicity Analysis of the A. terreus-Silica Composite

Phytotoxicity of CVD wastewater treated with *A. terreus*-silica composite was assessed using *Triticum aestivum* L. (wheat) grains, as shown in Figure 11. Seedling growth parameters, including germination percentage, plumule length, and radical numbers and length were measured. Treated CVD wastewater with silica-composite showed enhancing in the wheat grains germination comparing with the untreated CVD, was recorded 72% germination index (37% for untreated CVD, and 73% for water control), plumule length was 17.3 mm (13.3 mm for untreated CVD, and 17.7 mm for water control), radical length 46.3 mm (33.3 mm for untreated CVD and 36 mm for water control), while the number of branches were 5, 4, 5 and of radicals were 4, 3, 5 for water control, untreated CVD, and treated CVD, respectively as cleared in Figure 11.

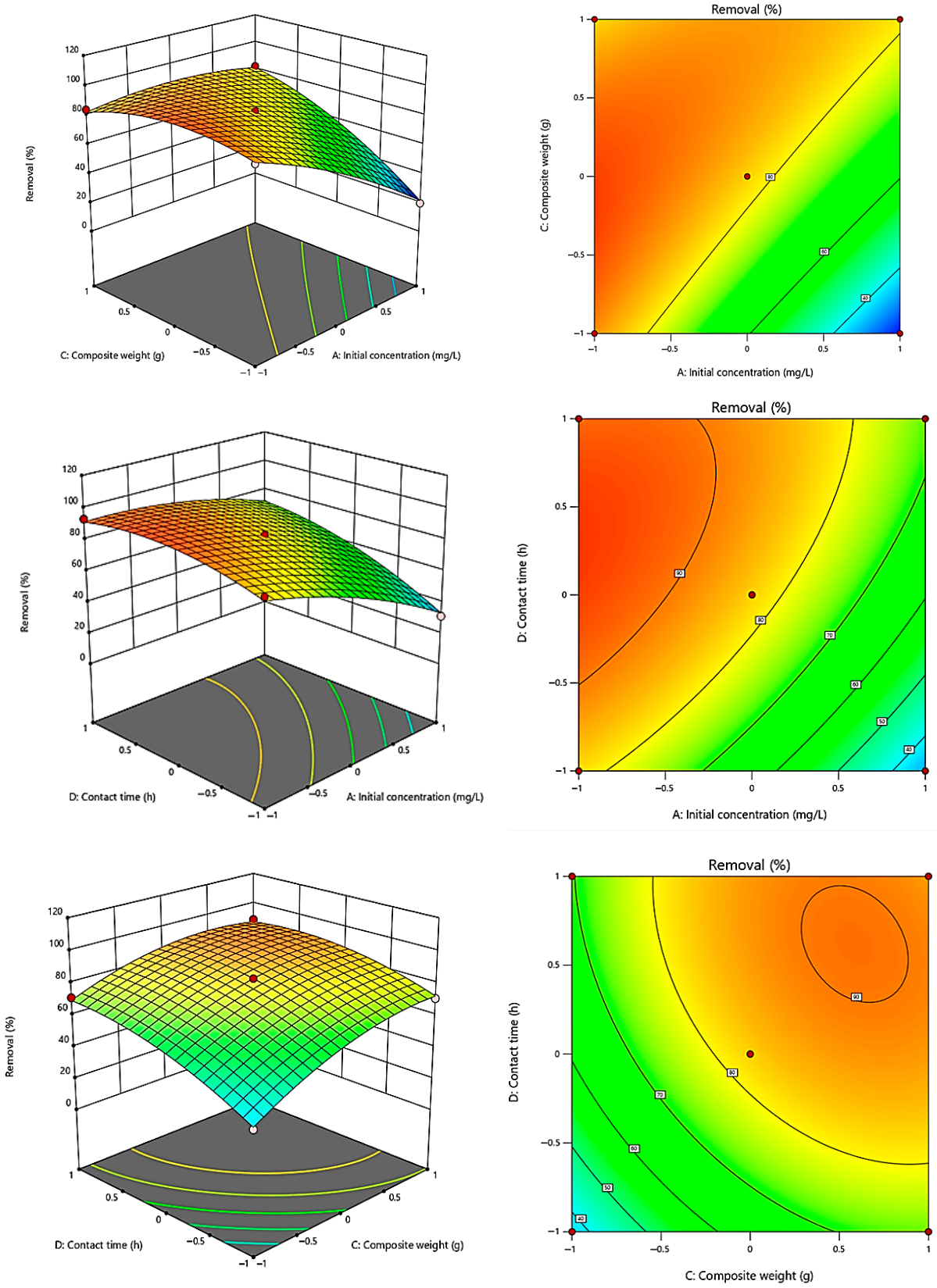


Figure 9. Box–Behnken statistical design 3D surface plots, clearing the interactions between AC (initial CVD concentration* adsorbent composite weight), AD (initial CVD concentration* contact time), CD (adsorbent composite weight* contact time) and their effects on the CVD removal (%) using *A. terreus*-silica composite.

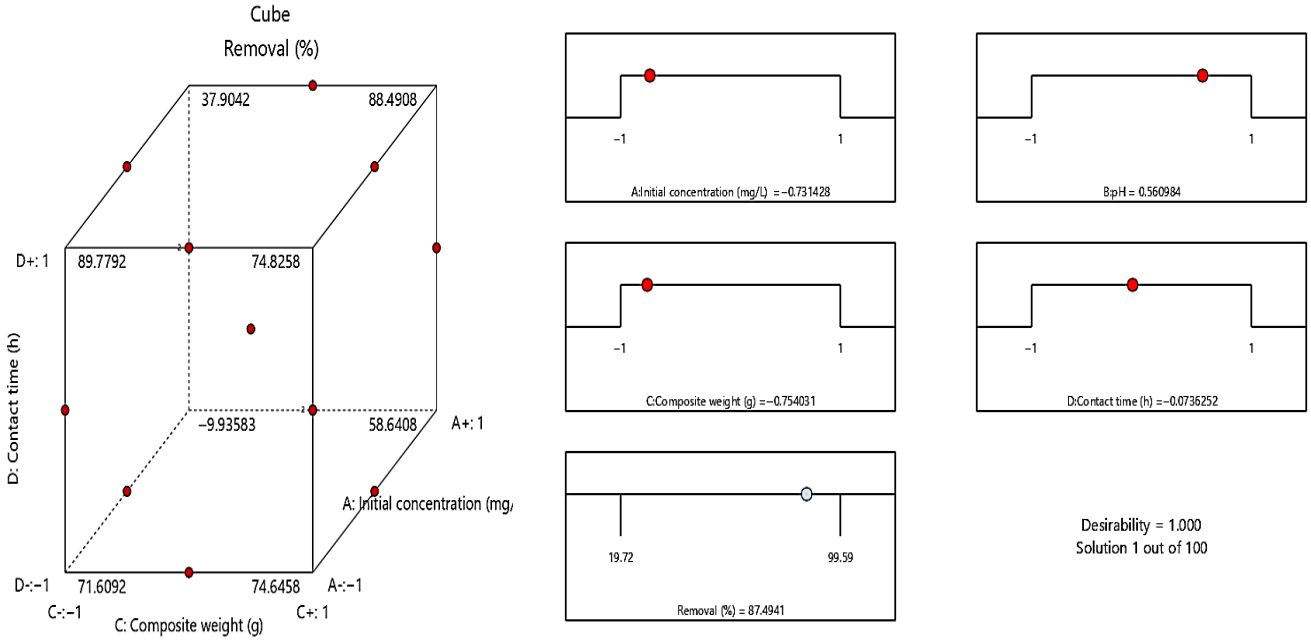


Figure 10. The statistical desirability ramp plot of CVD removal (%) using *A. terreus* silica composite.

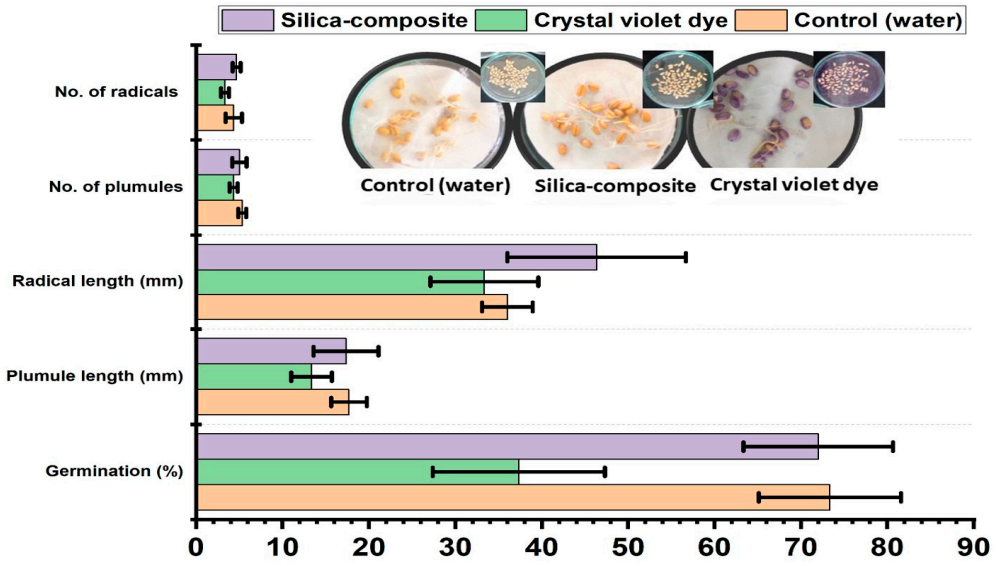


Figure 11. Phytotoxicity assay of treated (*A. terreus*-silica composite) and untreated (water dye solution) CVD on the germination of *Triticum aestivum* L. (wheat) as a grain plant model.

3.6. Microbial Toxicity Analysis of the A. terreus-Silica Composite

Microbial toxicity of CVD wastewater treated with *A. terreus*-silica composite was tested on the growth of *S. aureus*, *E. coli*, *K. pneumoniae*, *P. aeruginosa*, *C. albicans*, *A. flavus*, and *Aspergillus niger* using the well-diffusion method, as shown in Figure 12. The developed inhibition zones were measured in all treatments for each microbial strain. Results showed that the treated CVD water is non-toxic and has no toxicity activities to the tested bacteria, yeast, and filamentous fungi; however untreated CVD showed toxic activities to the microbial strains *S. aureus* (18 mm), *E. coli* (15 mm), *K. pneumoniae* (15 mm), *P. aeruginosa* (13 mm), *C. albicans* (13 mm), *A. flavus* (15 mm), and *Aspergillus niger* (14 mm) as cleared in Figure 12.

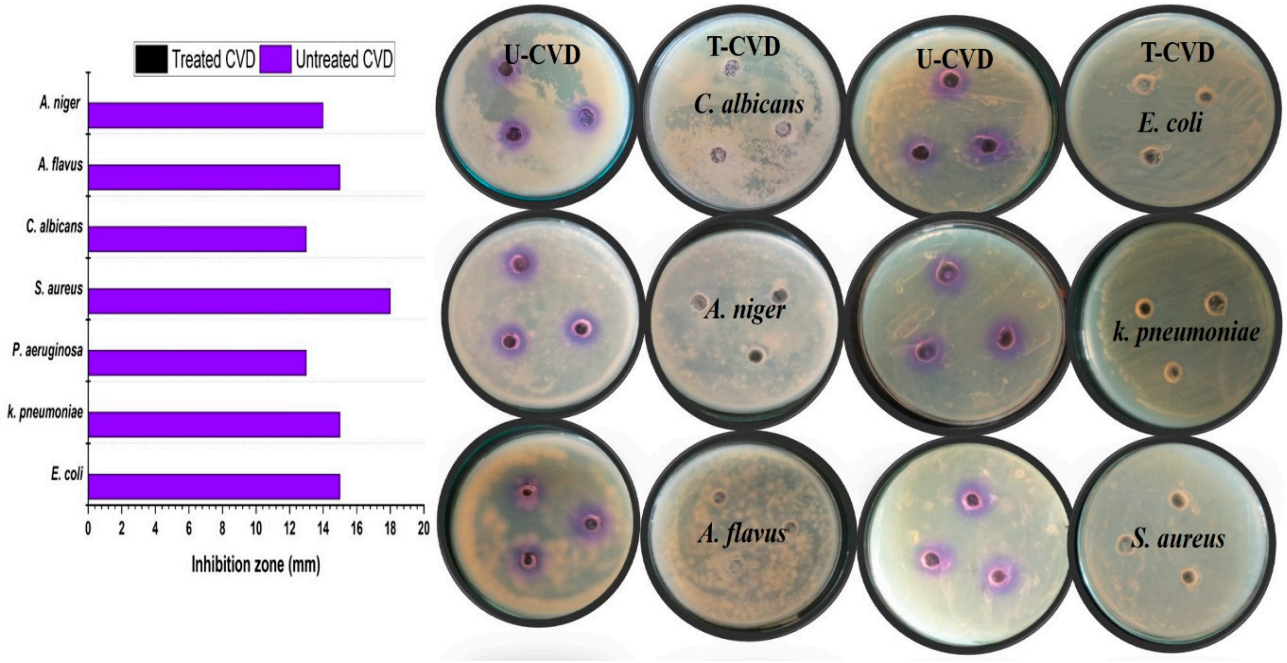


Figure 12. Microbial toxicity test of treated CVD using *A. terreus*-silica composite and untreated CVD solution at optimum removal conditions using *Escherichia coli*, *Klebsiella pneumoniae*, *Pseudomonas aeruginosa*, *Staphylococcus aureus*, *Candida albicans*, *Aspergillus flavus*, and *Aspergillus niger* tested strain.

3.7. Application of A. terreus-Silica Composite on Laboratory Real CVD Wastewater

Dyes wastewater with CVD collected from the bacteriological laboratory and treated with *A. terreus*-silica composite under the optimum parameters of Box–Behnken statistical design (BBD) showed 95.37%, in which the absorbance at 554 nm decreased from 2.0 (untreated wastewater) to 0.0925 (treated wastewater with *A. terreus*-silica composite) as shown in Figure 13. The composite proved its effectiveness in the adsorption of real wastewater, which recommends it as a sustainable tool for dye removal.

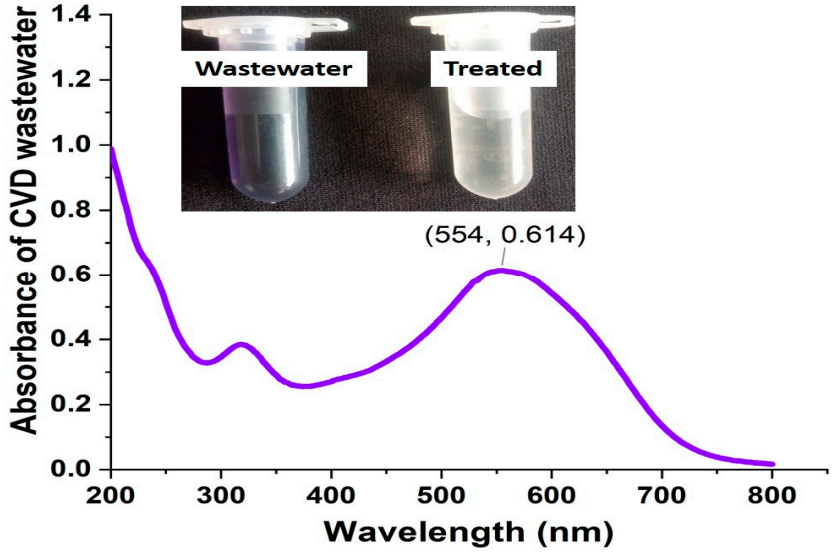


Figure 13. Application of *A. terreus*-silica composite in laboratory real CVD wastewater under the optimum parameters of Box–Behnken statistical design (BBD).

4. Discussion

Numerous industrial processes utilize hazardous synthetic compounds and subsequently discharge contaminated effluents, resulting in the pollution of the environmental

matrices [40]. Dyes were scored among the most common water pollutants for their widespread use across various industries such as textiles, food, plastics, and printing [41]. Dye-polluted water collected from the textile industries has unique microbial communities that can survive in harsh environments adapted to xenobiotic pollutants, which makes them superior sources for isolating dye-degrading fungi rather than unpolluted water sources [42,43]. Fungi could utilize these dyes as carbon and nitrogen sources, which gives them the ability to survive; they also have the ability to decolorize and degrade dyes through their enzymatic action [4,44]. *Aspergillus terreus* (PX920301) was recovered from textile wastewater. Previous studies showed that *Aspergillus* was the most dominant genus frequently isolated from dye-contaminated waters [45], which reflects their ecological versatility and dominance in harsh environments. Moreover, several studies stated the textile dyes decolorizing efficiencies of *Aspergillus* species, including by *A. tamarii* [46], *A. ochraceus* [47], brilliant green dye degraded by *Aspergillus* sp. [48], *A. niger* [49], *A. terreus* and *A. flavus* [50].

Aspergillus terreus-silica composite showed the highest CVD removal percentage by 85.4%, adsorption capacity (qe) 121.1 mg/L, and lowest CVD residual by 7.26 mg/L, compared with the DA-mycelia with CVD removal 40.23%, adsorption capacity (qe) 57.05 mg/L and CVD residual by 29.73 mg/L. Fungal mycelia-based composites are emerging as sustainable, low-cost materials for the removal of various pollutants from water and soil. These composites were previously prepared by growing filamentous fungi (*Pleurotus ostreatus*, *Ganoderma lucidum*, *Aspergillus* sp., and *Penicillium* spp.) on lignocellulosic or even agricultural-waste substrates until the mycelium fully colonizes the matrix, and then, after drying, the composite will have surface functionality [51,52]. The mycelial network provides abundant functional groups (-OH, -COOH, -NH_2) that bind pollutants via adsorption [20,51]. When combined with other functional additives, the fungal mycelia enhanced the adsorption capacity and removal kinetics [53], making them promising candidates for scalable, eco-friendly bioremediation systems. *Aspergillus*-mycelia-based systems represent low-cost, scalable, and can be adapted to packed-bed or immobilized-cell reactors, and they can also be utilized in dye decolorization [54]. Moreover, because *Aspergillus* is already used in industrial enzyme production, its deployment for the azo dye treatment could align with the existing industrial fermentation infrastructure [21,55].

The composite of *A. terreus*-silica composite showed combined FTIR bands from both dried *A. terreus* and silica oxide, including 3416.42 cm^{-1}, 2929.947 cm^{-1}, 2859.555 cm^{-1}, 1628.659 cm^{-1}, 1114.701 cm^{-1}, and 1018.756 cm^{-1}, which confirmed the formation of the composite. The fungus bands appeared in the region of 3600–3000 cm^{-1}, referred to the O–H (carbohydrates) and N–H (proteins/amide A), region of 2920–2850 cm^{-1} showed C–H stretching of lipids and aliphatic chains in fungi [56]. However, region 1650–1540 cm^{-1} represents the fungal protein backbone [56–58]. The dried *A. terreus* also showed a band at 1448.34 cm^{-1}, the bands in the region 1450–1400 cm^{-1} referred to C–H bending and CH_2/CH_3 deformation (lipids, proteins) [56]. Moreover, bands appeared in the region 1240–1000 cm^{-1} represented C–O and C–O–C stretching of polysaccharides (cell-wall mannans, glucans). All previous regions represent a fungal fingerprint that can be used for strain discrimination and monitoring the mycelial changes [59]. Moreover, silica oxide showed sharing bands with *A. terreus* mycelia- silica composite, including 1114.701 cm^{-1}, which is inside the region of 1200–1000 cm^{-1}, indicating (Si–O–Si) asymmetric stretching of the silica network. These peaks are often around 1080–1100 cm^{-1}, which is used as a fingerprint for the silica framework [60]. The absorption in the region 900–650 cm^{-1} is attributable to the sulphate group [61].

Fourier-transform infrared (FTIR) spectra of treated CVD with *A. terreus* mycelia silica composite showed new peaks at 2856.104 cm^{-1}, 1749.147 cm^{-1}, 1643.08 cm^{-1},

1558.226 cm^{-1}, 1459.872 cm^{-1} and 723.1865 cm^{-1}. These peaks confirmed the adsorption of the CVD on the composite. The CVD reported to have significant peaks at 1635–1731 cm^{-1}, clearing C=C stretching or C=O peaks correspond to its aromatic rings and triphenylmethane backbone, and recorded as a fingerprint band for CVD aromatic rings [62]. Around 1350–1370 cm^{-1} cleared C–N stretching vibrations of the aromatic tertiary amine groups (central carbon–N bonds). Also, C-O or S=O peaks cleared at 1000–1400 cm^{-1} and could also be shifted due to the electrostatic or complexation with sulfonic/carboxyl sites [63]. Around 2800–3000 cm^{-1}, there is a clear weak C–H stretching of methyl groups, which is shown as a broad band. FTIR peak shifting in CVD adsorption onto the composite adsorbents indicates interactions between the dye's functional groups and the adsorbent surface, confirming adsorption mechanisms like hydrogen bonding, electrostatic attraction, and complexation [64].

Optimizing CVD removal entails systematically adjusting key operational parameters and selecting appropriate adsorbent concentration to maximize both efficiency and capacity. Optimizing the CVD removal process using BBD design showed that the maximum CVD removal (%) was 99.59% obtained using 200 mg/L CVD, pH (8), 0.1 g/10 mL adsorbent composite weight during 48 h contact time. Moreover, dyes wastewater with CVD were treated with silica-composite under the optimum parameters of BBD design and showed 95.37% dyes removal. Comparing with our composite removal efficiencies of CVD, Kyi et al. [65] stated that the palm kernel biochar composite has a maximum adsorption of CVD 24.45 mg/g using one gram of the adsorbent. Foroutan et al. [35] utilized lemon wood nanocomposite for CVD adsorption and obtained a maximum adsorption by 98.3%. Mycelium-reinforced nanofiber was utilized for dyes filtration (astra blue and safranin) by Heide et al. [66]. *Pleurotus*-bagasse composite was utilized to remove lanasyn olive (textile dye) with 90% removal efficiencies [67]. Yanto et al. [68] found that the fungal mycelial-light clay composite has dyes decolorization efficiencies reach to 96%. Ani et al. [69] recorded a maximum CVD removal 90.04% using a 50 mg/L biochar composite. Mehta et al. [70] reached CVD removal >95% using seablite biochar-ferrite composite using pH 8, 30 mg adsorbent, and 200 mg/L CVD. Peighambardoust et al. [71] recorded CVD removal 98.54% using pH 9, nanocomposite biochar adsorbent 1 g/L, in a contact time of 70 min, using an initial CVD concentration of 10 mg/L. Moreover, many studies report CVD maximum removal around neutral–alkaline pH conditions, where electrostatic attraction between negative functional groups on the adsorbent and the positively charged CV is strongest. AL-Shehri et al. [64] reported that pH 9 was the best for CVD removal, Mahgoub et al. [72] reported that pH 8 was the optimum, while Sen et al. [73] reported that pH 6 was the optimum for CVD removal. These pH optimum changes could be related to the adsorbent type and composition. Low-cost materials represented the best choice for dye removal for their possible applicability in large-scale production [74–76]. Moreover, the efficiencies of various composites compared with our findings were clarified in Table 3.

Phytotoxicity of CVD wastewater treated with *A. terreus*-silica composite using *Triticum aestivum* L. (wheat) grains showed an enhancement in the wheat grains germination (72%) compared with the untreated CVD (37%), which was also near the control (water treated) treatment (73%). In agreement with our findings, CVD exhibits significant phytotoxicity to sorghum (*Sorghum bicolor*), inhibiting seed germination and seedling growth in various plants at concentrations as low as 0.00025 mg/mL to 100 mg/L [90]. Bharagava et al. [91] stated that CVD reduced the seed germination of *Phaseolus mungo* L. to 46.67%. At a concentration of 100 mg/L, CVD significantly inhibited the germination of *Triticum aestivum* (42%) and *Vigna radiata* (51%) [11]. Treated CVD water with *A. terreus*-silica composite has no toxicity activities to *S. aureus*, *E. coli*, *K. pneumoniae*, *P. aeruginosa*, *C. albicans*, *A. flavus*, and *Aspergillus niger*, while untreated CVD showed toxic activities

to all the microbial strains. Moreover, CVD has a triphenylmethane cationic structure that exhibits notable microbial toxicity, which makes it act as a bacteriostatic agent at low concentrations. Their mechanism of toxicity includes cell membrane disruption, respiration disturbance, and genotoxic impacts via DNA intercalation and generation of oxidative stress [10,13]. Treated CVD shows markedly reduced microbial toxicity compared to its untreated form, as adsorption chelates the dye into the adsorbent, breaks it down into less harmful metabolites, or adsorbs the dye from the water [11,13].

Table 3. Efficiencies of various composites in removing crystal violet dye.

Composite Type	Adsorbent Material	Removal (%) or qm (mg/g)	Reference
Biomass-derived composites	Pomegranate peel	Maximum removal capacities of 675.47 mg/g (PPP/Sn–Fe) and 357.18 mg/g (PPP/Sn–Zn)	[77]
	Pine needles–PANI	Maximum removal capacities under optimized conditions 327 mg/g.	[78]
	Sugarcane bagasse	72.09% removal of CVD, qm 77.22 mg/g	[79]
Clay-based composites	Bentonite/MgO	12% increasing of CVD removal, qm 423.02 mg/g	[80]
Fungal composite	*A. terreus*-silica composite	99.59% removal of CVD in real wastewater	Our study
	Trichoderma–graphene oxide aerogel	97% removal of CVD	[81]
	Immobilized *Actinomucor elegans* mass	96.4% removal of CVD	[82]
	Trametes versicolor—rice husk	97% removal of CVD	[83]
Carbon-based composites	rGO-ED@Cellulose	260 mg/g CVD adsorption capacity	[84]
	Palm kernel biochar	Maximum adsorption of CVD 24.45 mg/g	[65]
	Biochar	Maximum CVD removal 90.04%	[69]
	Seablite biochar-ferrite	CVD removal >95%	[70]
MOF-based composites	Fe-MOF/alginate hybrids	1334 mg/g CVD adsorption capacity	[85]
ZIF-based composites	ZIF-8/graphene quantum dot	7162 mg/g adsorption capacity	[86]
Hydrogels and polymeric composites	Pectin–pullulan–kaolinite	93.8% CVD removal, 205.57 mg/g adsorption capacity	[87]
	Fe_3O_4/Poly(acrylic acid)	95% CVD removal, 321 mg/g adsorption capacity	[88]
Peptoid-based fibrils	N-aryl pseudo-peptoid fibrils	666 mg/g adsorption capacity	[89]

5. Conclusions

In conclusion, the present study demonstrates that the developed *Aspergillus terreus*-silica composite represents a highly efficient, sustainable, and environmentally safe adsorbent for the removal of CVD from aqueous systems. The composite significantly enhanced adsorption performance compared to active dried fungal mycelia alone, achieving high removal efficiency and adsorption capacity under optimized conditions. Statistical optimization using the Box–Behnken design confirmed maximum dye removal under optimized conditions, highlighting the robustness and reliability of the process. Furthermore, the composite exhibited negligible phytotoxicity and no microbial toxicity effects, indicating its biosafety for environmental applications. Its effective performance in treating

real dye-contaminated wastewater further validates its practical applicability. Overall, this study provides strong evidence that fungal–inorganic composites can serve as cost-effective and eco-friendly alternatives for the bioremediation of hazardous azo dye pollutants in industrial effluents. Future research should focus on scaling up the application of the *Aspergillus terreus*-silica composite for pilot- and industrial-scale wastewater treatment systems, with particular emphasis on continuous-flow operations. Further studies are recommended to evaluate the regeneration, reusability, and long-term stability of the composite to enhance its economic feasibility, especially in real field conditions (i.e., real wastewater treatment plants). Integration with other treatment technologies, like membrane filtration, could further improve removal efficiency.

Author Contributions: Conceptualization, G.A.-E.M.; methodology, R.M.F.; software, G.A.-E.M. and R.M.F.; validation, G.A.-E.M.; formal analysis, G.A.-E.M. and R.M.F.; investigation, G.A.-E.M. and R.M.F.; resources, G.A.-E.M. and R.M.F.; data curation, G.A.-E.M.; writing—original draft preparation, G.A.-E.M. and R.M.F.; writing—review and editing, G.A.-E.M. and A.Y.A.-M.; supervision, G.A.-E.M. and A.Y.A.-M.; project administration, G.A.-E.M.; funding acquisition, G.A.-E.M. All authors have read and agreed to the published version of the manuscript.

Funding: This research received no external funding.

Institutional Review Board Statement: Not applicable.

Informed Consent Statement: Not applicable.

Data Availability Statement: The datasets used and/or analyzed during the current study are available from the corresponding author on reasonable request. Sequence data that support the findings of this study have been deposited in the NCBI with the accession code *A. terreus* (Accession no. PX920301) (https://www.ncbi.nlm.nih.gov/nuccore/PX920301.1) (accessed on 13 January 2026).

Acknowledgments: The authors are grateful for the insightful, constructive suggestions and careful corrections made by the Editor and the reviewers for the improvements of this manuscript.

Conflicts of Interest: The authors declare no conflicts of interest.

References

1. Mahmoud, G.A.-E.; Thakur, N.; Hefzy, M. Responses of Marine Fungi to Heavy Metal Contamination. In *Current Status of Marine Water Microbiology*; Soni, R., Suyal, D.C., Morales-Oyervides, L., Fouillaud, M., Eds.; Springer: Singapore, 2023; pp. 263–277. [CrossRef]
2. Mahmoud, G.A.E.; Taher, E.M.; Zeinab, I.A.; Ahmed, L.I.; Khalefa, H.S. Insights on Wastewater Impacts on Animal Health and Production. In *Microbial Applications in Industrial Wastewater Treatment: Advances in Wastewater Research*; Dey, S., Shah, M.P., Eds.; Springer: Singapore, 2026. [CrossRef]
3. Khamparia, S.; Jaspal, D. Technologies for Treatment of Colored Wastewater from Different Industries. In *Handbook of Environmental Materials Management*; Hussain, C.M., Ed.; Springer Publishing: Cham, Switzerland, 2018. [CrossRef]
4. Berradi, M.; Hsissou, R.; Khudhair, M.; Assouag, M.; Cherkaoui, O.; El Bachiri, A.; El Harfi, A. Textile finishing dyes and their impact on aquatic environs. *Heliyon* **2019**, *5*, e02711. [CrossRef]
5. Ajaz, M.; Shakeel, S.; Rehman, A. Microbial use for azo dye degradation-a strategy for dye bioremediation. *Int. Microbiol.* **2020**, *23*, 149–159. [CrossRef]
6. Zafar, S.; Bukhari, D.A.; Rehman, A. Azo dyes degradation by microorganisms—An efficient and sustainable approach. *Saudi J. Biol. Sci.* **2022**, *29*, 103437. [CrossRef]
7. Shi, Y.; Yang, Z.; Xing, L.; Zhang, X.; Li, X.; Zhang, D. Recent advances in the biodegradation of azo dyes. *World J. Microbiol. Biotechnol.* **2021**, *37*, 137. [CrossRef]
8. Abd El-latif, A.S.; Zohri, A.N.A.; El-Aref, H.M.; Mahmoud, G.A.-E. Kinetic studies on optimized extracellular laccase from Trichoderma harzianum PP389612 and its capabilities for azo dye removal. *Microb. Cell Fact.* **2024**, *23*, 150. [CrossRef]
9. Azmi, W.; Sani, R.K.; Banerjee, U.C. Biodegradation of triphenylmethane dyes. *Enzym. Microb. Technol.* **1998**, *22*, 185–191. [CrossRef] [PubMed]
10. Mani, S.; Bharagava, R.N. Exposure to Crystal Violet, Its Toxic, Genotoxic and Carcinogenic Effects on Environment and Its Degradation and Detoxification for Environmental Safety. *Rev. Environ. Contam. Toxicol.* **2016**, *237*, 71–104. [CrossRef] [PubMed]

11. Tian, Y.; Wu, K.; Lin, S.; Shi, M.; Liu, Y.; Su, Y.; Islam, R. Biodegradation and Decolorization of Crystal Violet Dye by Cocultivation with Fungi and Bacteria. *ACS Omega* **2024**, *9*, 7668–7678. [CrossRef] [PubMed]
12. Filice, S.; Scuderi, V.; Scalese, S. Sulfonated Pentablock Copolymer (NexarTM) for Water Remediation and Other Applications. *Polymers* **2024**, *16*, 2009. [CrossRef]
13. Kwak, S.J.; Park, J.; Sim, Y.; Choi, H.; Cho, J.; Lee, Y.M. Biodegradation of crystal violet by newly isolated bacteria. *PeerJ* **2024**, *12*, e17442. [CrossRef]
14. Homagai, P.L.; Poudel, R.; Poudel, S.; Bhattarai, A. Adsorption and removal of crystal violet dye from aqueous solution by modified rice husk. *Heliyon* **2022**, *8*, e09261. [CrossRef]
15. Mahmoud, G.A.-E.; Kumar, B. (Eds.) *Microbial Solutions for Sustainable Agriculture*, 1st ed.; CRC Press: Boca Raton, FL, USA, 2025. [CrossRef]
16. El Naeem, G.A.; Abd-Elhamid, A.; Farahat, O.O.; El-Bardan, A.A.; Soliman, H.M.; Nayl, A. Adsorption of crystal violet and methylene blue dyes using a cellulose-based adsorbent from sugercane bagasse: Characterization, kinetic and isotherm studies. *J. Mater. Res. Technol.* **2022**, *19*, 3241–3254. [CrossRef]
17. Gandia, A.; van den Brandhof, J.G.; Appels, F.V.W.; Jones, M.P. Flexible fungal materials: Shaping the future. *Trends Biotechnol.* **2021**, *39*, 1321–1331. [CrossRef] [PubMed]
18. Aksu, Z.; Tatli, A.Í.; Tunç, Ö. A comparative adsorption/biosorption study of Acid Blue 161: Effect of temperature on equilibrium and kinetic parameters. *Chem. Eng. J.* **2008**, *142*, 23–39. [CrossRef]
19. Mahmoud, G.A.-E. Microbial Scavenging of Heavy Metals Using Bioremediation Strategies. In *Rhizobiont in Bioremediation of Hazardous Waste*; Kumar, V., Prasad, R., Kumar, M., Eds.; Springer: Singapore, 2021; pp. 265–289. [CrossRef]
20. Aiduang, W.; Chanthaluck, A.; Kumla, J.; Jatuwong, K.; Srinuanpan, S.; Waroonkun, T.; Oranratmanee, R.; Lumyong, S.; Suwannarach, N. Amazing Fungi for Eco-Friendly Composite Materials: A Comprehensive Review. *J. Fungi* **2022**, *8*, 842. [CrossRef] [PubMed]
21. Li, K.; Jia, J.; Wu, N.; Xu, Q. Recent advances in the construction of biocomposites based on fungal mycelia. *Front. Bioeng. Biotechnol.* **2022**, *10*, 1067869. [CrossRef]
22. Yang, L.; Park, D.; Qin, Z. Material function of mycelium-based biocomposite: A review. *Front. Mater.* **2021**, *8*, 737377. [CrossRef]
23. Zhang, X.J.; Hu, J.Y.; Fan, X.D.; Yu, X. Naturally grown mycelium composite as sustainable building insulation materials. *J. Clean. Prod.* **2022**, *342*, 130784. [CrossRef]
24. Marszałek, A.; Puszczało, E.; Szymańska, K.; Sroka, M.; Kudlek, E.; Generowicz, A. Application of Mesoporous Silicas for Adsorption of Organic and Inorganic Pollutants from Rainwater. *Materials* **2024**, *17*, 2917. [CrossRef]
25. Flores, D.; Almeida, C.M.R.; Gomes, C.R.; Balula, S.S.; Granadeiro, C.M. Tailoring of Mesoporous Silica-Based Materials for Enhanced Water Pollutants Removal. *Molecules* **2023**, *28*, 4038. [CrossRef]
26. Hafidi, E.M.E.; Mortadi, A.; Graich, A.; Chahid, E.; Laasri, S.; El Moznine, R.; Monkade, M. Monitoring treatment of industrial wastewater using conventional methods and impedance spectroscopy. *Environ. Monit. Assess.* **2023**, *195*, 832. [CrossRef]
27. Zeb, S.; Ali, N.; Ali, Z.; Bilal, M.; Adalat, B.; Hussain, S.; Gul, S.; Ali, F.; Ahmad, R.; khan, S.; et al. Silica-based nanomaterials as designer adsorbents to mitigate emerging organic contaminants from water matrices. *J. Water Process Eng.* **2020**, *38*, 101675. [CrossRef]
28. Yang, C.; Liu, N.; Guo, X.; Qiao, C. Cloning of mpd gene from a chlorpyrifos-degrading bacterium and use of this strain in bioremediation of contaminated soil. *FEMS Microbiol. Lett.* **2006**, *265*, 118–125. [CrossRef] [PubMed]
29. Raper, K.B.; Fennell, D.I. *The Genus Aspergillus*; Williams and Wilkins: Baltimore, MD, USA, 1965; p. 686.
30. Moubasher, A.H. *Soil Fungi in Qatar and Other Arab Countries*; Univeristy of Qatar, Centre for Scientific and Applied Research: Doha, Qatar, 1993; p. 566.
31. White, T.J.; Bruns, T.; Lee, S.; Taylor, J. Amplification and direct sequencing of fungal ribosomal RNA genes for phylogenetics. In *PCR Protocols: A Guide to Methods and Applications*; Innis, M.A., Gelfand, D.H., Sninsky, J.J., White, T.J., Eds.; Academic Press: San Diego, CA, USA, 1990; pp. 315–322.
32. Mahmoud, G.A.-E.; Abdel-Sater, M.A.; Al-Amery, E.; Hussein, N.A. Controlling Alternaria cerealis MT808477 Tomato Phytopathogen by Trichoderma harzianum and Tracking the Plant Physiological Changes. *Plants* **2021**, *10*, 1846. [CrossRef] [PubMed]
33. Thompson, J.D.; Higgins, D.G.; Gibson, T.J. CLUSTAL W: Improving the sensitivity of progressive multiple sequence alignment through sequence weighting, position-specific gap penalties and weight matrix choice. *Nucleic Acids Res.* **1994**, *22*, 4673–4680. [CrossRef]
34. Pan, X.; Zuo, G.; Su, T.; Cheng, S.; Gu, Y.; Qi, X.; Dong, W. Polycarboxylic magnetic polydopamine sub-microspheres for effective adsorption of malachite green. *Colloid Surf.* **2019**, *560*, 106–113. [CrossRef]
35. Foroutan, R.; Peighambardoust, S.J.; Peighambardoust, S.H.; Pateiro, M.; Lorenzo, J.M. Adsorption of Crystal Violet Dye Using Activated Carbon of Lemon Wood and Activated Carbon/Fe_3O_4 Magnetic Nanocomposite from Aqueous Solutions: A Kinetic, Equilibrium and Thermodynamic Study. *Molecules* **2021**, *26*, 2241. [CrossRef]

36. Mahmoud, G.A.-E.; Abdel Shakor, A.; Kamal-Eldin, N.A.; Zohari, A. Production of kojic acid by Aspergillus flavus OL314748 using box-Behnken statistical design and its antibacterial and anticancer applications using molecular docking technique. *BMC Microbiol.* **2024**, *24*, 140. [CrossRef]
37. Liu, H.; Wang, K.; Schlindwein, W.; Li, M. Using the Box–Behnken experimental design to optimise operating parameters in pulsed spray fluidised bed granulation. *Int. J. Pharm.* **2013**, *448*, 329–338. [CrossRef]
38. Fouda, A.; Hassan, S.E.; Saied, E.; Hamza, M.F. Photocatalytic degradation of real textile and tannery effluent using biosynthesized magnesium oxide nanoparticles (MgO-NPs), heavy metal adsorption, phytotoxicity, and antimicrobial activity. *J. Environ. Chem. Eng.* **2021**, *9*, 105346. [CrossRef]
39. Mahmoud, G.A.E.; Sabra, M.A.; Mohamed, A.E.; Darwish, K.M.; Gaber, D.A. Optimization of Gibberellic Acid Production from Fusarium incarnatum and Its Effect on Zea mays Growth Promotion and Antioxidant Activity. *J. Plant Growth Regul.* **2025**, *44*, 3219–3235. [CrossRef]
40. Mahmoud, G.A.E.; Badawy, M.S.; Bougafa, F.H.E.; Barakat, H.M.; Ahmed, L.I. Chapter 3—Environmental risks of plastics pollutants and their mycoremediation strategies. In *Development in Wastewater Treatment Research and Processes, Microbial Biotechnology: Integrated Microbial Engineering for B3—Bioenergy, Bioremediation, and Bioproducts*; Shah, M.P., Bala, K., Eds.; Elsevier: Amsterdam, The Netherlands, 2025; pp. 69–89. [CrossRef]
41. Khan, I.; Saeed, K.; Zekker, I.; Zhang, B.; Hendi, A.H.; Ahmad, A.; Ahmad, S.; Zada, N.; Ahmad, H.; Shah, L.A.; et al. Review on methylene blue: Its properties, uses, toxicity and photodegradation. *Water* **2022**, *14*, 242. [CrossRef]
42. El Hafidi, E.M.; Mortadi, A.; Lizoul, B.; Hairch, Y.; Mghaiouini, R.; Sabor, A.; Mnaouer, K.; Chahid, E.; Jebbari, S.; El Moznine, R.; et al. Assessment of sand and hearth ash filtration for wastewater treatment and novel monitoring via complex conductivity. *Euro-Mediterr. J. Environ. Integr.* **2025**, *10*, 1137–1148. [CrossRef]
43. Gizaw, B.; Alemu, T.; Ebsa, G. Screening and identification of microbes from polluted environment for azodye (Turquoise blue) decolorization. *Heliyon* **2024**, *10*, e32769. [CrossRef]
44. Mahmoud, G.A.E.; Ahmed, L.I.; Bougafa, F.H.E.; Barakat, H.M.; Nofal, A.S.; Badawy, M.S.E.M. Unique Enzymatic Power of Microbial Cleaners During the Soil Bioremediation Process. In *Soil Bioremediation: Environmental Science and Engineering*; Shah, M.P., Deka, D., Eds.; Springer: Cham, Switzerland, 2025. [CrossRef]
45. Rajhans, G.; Barik, A.; Sen, S.K.; Raut, S. Degradation of dyes by fungi: An insight into mycoremediation. *Biotechnologia* **2021**, *102*, 445–455. [CrossRef]
46. Ramalingam, S.; Saraswathy, N.; Shanmugapriya, S.; Shakthipriyadarshani, S.; Sadasivam, S.; Sanmugaprakash, M. Decolorization of textile dyes by Aspergillus tamari, mixed fungal culture and Peniceillium purpurogenum. *J. Scien Ind. Res.* **2010**, *69*, 151–153.
47. Tisma, M.; Komar, M.; Rajic, M.; Pavlovic, H.; Zelic, B. Decolorization of dyes by Aspergillus Ochraceus cultivated under solid state fermentation on sugar beet waste. *Chem. Eng. Trans.* **2012**, *27*, 62–67. [CrossRef]
48. Kumar, C.G.; Mongolla, P.; Joseph, J.; Sarma, V.U.M. Decolorization and biodegradation of triphenylmethane dye, brilliant green, by Aspergillus sp. isolated from Ladakh, India. *Process Biochem.* **2012**, *47*, 1388–1394. [CrossRef]
49. Lira Pérez, J.; Rodríguez Vázquez, R. Removal of orange G dye by Aspergillus niger and its effect on organic acid production. *Prep. Biochem. Biotechnol.* **2023**, *53*, 860–871. [CrossRef]
50. Ghanaim, A.M.; Mahdy, O.M.E.; Mohamed, H.I. Biodegradation of azo dyes by Aspergillus flavus and its bioremediation potential using seed germination efficiency. *BMC Microbiol.* **2025**, *25*, 7. [CrossRef]
51. Zhou, H.; Li, X.; Hu, B.; Wu, M.; Zhang, Y.; Yi, X.; Liu, Y. Assembly of fungal mycelium-carbon nanotube composites and their application in pyrene removal. *J. Hazard. Mater.* **2021**, *415*, 125743. [CrossRef] [PubMed]
52. Barta, D.G.; Simion, I.; Tiuc, A.E.; Vasile, O. Mycelium-Based Composites as a Sustainable Solution for Waste Management and Circular Economy. *Materials* **2024**, *17*, 404. [CrossRef] [PubMed]
53. Camilleri, E.; Narayan, S.; Lingam, D.; Blundell, R. Mycelium-based composites: An updated comprehensive overview. *Biotechnol. Adv.* **2025**, *79*, 108517. [CrossRef] [PubMed]
54. de Castro, K.C.; Leme, V.F.C.; Souza, F.H.M.; Costa, G.O.B.; Santos, G.E.; Litordi, L.R.V.; Andrade, G.S.S. Performance of inactivated Aspergillus oryzae cells on dye removal in aqueous solutions. *Environ. Technol. Innov.* **2021**, *24*, 101828. [CrossRef]
55. Alihosseini, F.S.; Azimi, H.; Mostajeran, M.; Feiz, M. Removal of different vat dyes by Aspergillus niger: A comparative study focusing on the molecular structure. *J. Microbiol. Methods* **2023**, *208*, 106720. [CrossRef]
56. Tralamazza, S.M.; Bozza, A.; Destro, J.G.R.; Rodríguez, J.I.; Dalzoto, P.R.; Pimentel, I.C. Potential of Fourier Transform Infrared Spectroscopy (FT-IR) to Differentiate Environmental Aspergillus Fungi Species A. niger, A. ochraceus, and A. westerdijkiae Using Two Different Methodologies. *Appl. Spectrosc.* **2013**, *67*, 274–278. [CrossRef]
57. Naumann, A. novel procedure for strain classification of fungal mycelium by cluster and artificial neural network analysis of Fourier transform infrared (FTIR) spectra. *Analyst* **2009**, *134*, 1215–1223. [CrossRef]
58. Dróżdż, A.; Kubera, D.; Olender, A.; Dabrowski, W.; Szukala, M.; Wosko, S.; Chwiej, J.; Rugiel, M.; Kawoń, K.; Gagoś, M. ATR-FTIR spectroscopic markers indicating drug resistance in selected Candida strains. *Sci. Rep.* **2025**, *15*, 18130. [CrossRef]

59. Abu-Aqil, G.; Adawi, S.; Huleihel, M. Early and swift identification of fungal-infection using infrared spectroscopy. *Spectrochim. Acta Part A Mol. Biomol. Spectrosc.* **2025**, *325*, 125101. [CrossRef]
60. Ellerbrock, R.H.; Stein, M.; Schaller, J. Comparing silicon mineral species of different crystallinity using Fourier transform infrared spectroscopy. *Front. Environ. Chem.* **2024**, *5*, 1462678. [CrossRef]
61. Liu, C.; Ma, L.; Rao, Z.; Li, Y. Synthesis and thermal properties of magnesium sulfate heptahydrate/urea resin as thermal energy storage micro-encapsulated phase change material. *J. Heat Mass Transf.* **2018**, *140*, 014501. [CrossRef]
62. Imran, M.S.; Javed, T.; Areej, I.; Haider, M.N. Sequestration of crystal violet dye from wastewater using low-cost coconut husk as a potential adsorbent. *Water Sci. Technol.* **2022**, *85*, 2295–2317. [CrossRef] [PubMed]
63. Huang, Y.-P.; Niu, H.-B.; Jin, L.; Jiao, L.; Johnson, D.; Tian, H.-L.; Sarina, S.; Zhu, H.-Y.; Fang, Y.-F. Selective adsorption of Crystal Violet via hydrogen bonded water bridges by InVO4. *Chem. Eng. J. Adv.* **2023**, *15*, 100508. [CrossRef]
64. AL-Shehri, H.S.; Almudaifer, E.; Alorabi, A.Q.; Alanazi, H.S.; Alkorbi, A.S.; Alharthi, F.A. Effective adsorption of crystal violet from aqueous solutions with effective adsorbent: Equilibrium, mechanism studies and modeling analysis. *Environ. Pollut. Bioavailab.* **2021**, *33*, 214–226. [CrossRef]
65. Kyi, P.P.; Quansah, J.O.; Lee, C.-G.; Moon, J.-K.; Park, S.-J. The Removal of Crystal Violet from Textile Wastewater Using Palm Kernel Shell-Derived Biochar. *Appl. Sci.* **2020**, *10*, 2251. [CrossRef]
66. Heide, A.; Wiebe, P.; Sabantina, L.; Ehrmann, A. Suitability of Mycelium-Reinforced Nanofiber Mats for Filtration of Different Dyes. *Polymers* **2023**, *15*, 3951. [CrossRef]
67. Gita, S.; Shukla, S.P.; Deshmukhe, G.; Singh, A.R.; Choudhury, T.G. Adsorption linked fungal degradation process for complete removal of Lanasyn olive dye using chemically valorized sugarcane bagasse. *Waste Manag. Bull.* **2023**, *1*, 29–38. [CrossRef]
68. Yanto, D.H.Y.; Chempaka, R.M.; Nurhayat, O.D.; Argo, B.D.; Watanabe, T.; Wibisono, Y.; Hung, Y.T. Optimization of dye-contaminated wastewater treatment by fungal Mycelial-light expanded clay aggregate composite. *Environ. Res.* **2023**, *231*, 116207. [CrossRef]
69. Ani, M.O.; Menkiti, M.C.; Aniagor, C.O.; Nworie, C.E.; Ochi, D.O. Canarium Schweinfurthii Stone-Derived Biochar: A Promising Adsorbent for Crystal Violet Dye Removal. *Results Surf. Interfaces* **2023**, *12*, 100144. [CrossRef]
70. Mehta, D.; Dave, P.N.; Kumar, V.V. Toxic crystal violet dye removal by novel, eco-friendly seablite biochar-ferrite composite: Adsorption isotherm, kinetics, and artificial neural network. *RSC Adv.* **2025**, *15*, 33189–33208. [CrossRef]
71. Peighambardoust, S.J.; Abdollahian Aghbolagh, S.; Foroutan, R.; Peighambardoust, N.S. Decontamination of Crystal Violet Using Nanocomposite Adsorbent Based on Pine Cone Biochar Modified with $CoFe_2O_4$/Mn-Fe LDH. *Sci. Rep.* **2025**, *15*, 15067. [CrossRef] [PubMed]
72. Mahgoub, S.M.; Alawam, A.S.; Allam, A.A.; Mahmoud, M.R.; Elrafey, A.; Abdelmohsen, A.H.; Mahmoud, R. Crystal violet removal from aqueous solution: Adsorption studies, Box-Behnken optimization, safety, and reuse in methanol oxidation. *RSC Adv.* **2025**, *15*, 44373–44391. [CrossRef] [PubMed]
73. Sen, N.; Shefa, N.R.; Reza, K. Adsorption of crystal violet dye from synthetic wastewater by ball-milled royal palm leaf sheath. *Sci. Rep.* **2024**, *14*, 5349. [CrossRef] [PubMed]
74. Filice, S.; Bongiorno, C.; Libertino, S.; Gradon, L.; Iannazzo, D.; Scalese, S. Photo-Fenton Degradation of Methyl Orange with Dunino Halloysite as a Source of Iron. *Catalysts* **2022**, *12*, 257. [CrossRef]
75. Filice, S.; Scuderi, V.; Libertino, S.; Zimbone, M.; Galati, C.; Spinella, N.; Gradon, L.; Falqui, L.; Scalese, S. Sulfonated Pentablock Copolymer Coating of Polypropylene Filters for Dye and Metal Ions Effective Removal by Integrated Adsorption and Filtration Process. *Int. J. Mol. Sci.* **2022**, *23*, 11777. [CrossRef]
76. Filice, S.; Bongiorno, C.; Libertino, S.; Compagnini, G.; Gradon, L.; Iannazzo, D.; La Magna, A.; Scalese, S. Structural Characterization and Adsorption Properties of Dunino Raw Halloysite Mineral for Dye Removal from Water. *Materials* **2021**, *14*, 3676. [CrossRef]
77. Hamrouche, N.; Djilani, C.; Belhocine, Y.; Bouzenad, N.; Amir, L.B.; Meradi, S.; Hamrouche, I.; Ben Ali, D.S. Comprehensive characterization and RSM-based optimization of crystal violet adsorption using $SnCl_2$–$FeCl_3$ and $SnCl_2$–$ZnCl_2$ activated pomegranate peel biosorbents. *RSC Adv.* **2026**, *16*, 4318–4334. [CrossRef]
78. Rana, S.; Chauhan, S. Designing etherified pine needles and polyaniline composite via epichlorohydrin linkage for highly efficient adsorption of cationic dyes. *Surf. Interfaces* **2026**, *83*, 108540. [CrossRef]
79. Tran-Nguyen, P.L.; Ly, K.P.; Dang, H.G.; Nguyen, M.-N.; Dang, V.-P.; Tran, N.-P.; Santoso, S.P.; Yuliana, M.; Angkawijaya, A.E.; Quyen, T.T.B.; et al. Effective removal of crystal violet in the aqueous solution using magnetic composites originated from sugarcane bagasse. *Chem. Pap.* **2025**, *79*, 2207–2223. [CrossRef]
80. Silva, P.F.; Fernandes, J.V.; Silva, V.C.; Filho, J.I.S.; Rodrigues, A.M.; Menezes, R.R.; Neves, G. Brazilian bentonite/MgO composites for adsorption of cationic and anionic dyes. *Environ. Sci. Pollut. Res.* **2024**, *31*, 58905–58927. [CrossRef]
81. Ali, S.S.M.; Al-Shammari, R.H.H.; Al-Mamoori, A.M.J. Removing Toxic Dyes from Aqueous Medium by Trichoderma-Graphain Oxide Aerogel. *Baghdad Sci. J.* **2023**, *20*, 18. [CrossRef]

82. Hasanien, Y.A.; Zaki, A.G.; Abdel-Razek, A.S. Employment of collective physical pretreatment and immobilization of Actinomucor biomass for prospective crystal violet remediation efficiency. *Biomass Convers. Biorefin.* **2025**, *15*, 3235–3249. [CrossRef]
83. Gutiérrez-Quirós, J.A.; Coronado-Marchena, A.; Villegas-Solano, D.; Rodríguez-Saravia, S.; Castro-Gutiérrez, V.; Rodríguez-Rodríguez, C.E. Improved productivity and dye removal performance of Trametes versicolor pellets using rice husk as a co-substrate. *J. Microbiol. Methods* **2024**, *223*, 106976. [CrossRef] [PubMed]
84. Zarrik, B.; El Amri, A.; Bensalah, J.; Jebli, A.; Lebkiri, A.; Hsissou, R.; Hbaiz, E.; Rifi, E.; Lebkiri, A. Adsorption of crystal violet using a composite based on graphene Oxide-ED@Cellulose: Adsorption modeling, optimization and recycling. *Inorg. Chem. Commun.* **2024**, *162*, 112179. [CrossRef]
85. Liang, P.; Ain, Q.; Dai, L.; Huang, K.; Huang, K.; Tong, Z. Eco-engineered sodium alginate-bentonite-Fe-ATA aerogels with tunable crosslinking for high-efficiency cationic dye adsorption. *Int. J. Biol. Macromol.* **2026**, *350*, 150997. [CrossRef]
86. Hussaini, M.; Onaizi, S.A.; Vohra, M.S. High-capacity removal of crystal violet using ZIF-8/graphene quantum dot composite with RSM optimization and explainable machine learning. *Sci. Rep.* **2026**, *16*, 9035. [CrossRef]
87. Nandal, K.; Jindal, R. Enhanced dye adsorption via pectin/pullulan/kaolinite nanocomposite for wastewater treatment applications. *Int. J. Biol. Macromol.* **2025**, *319*, 145557. [CrossRef]
88. Ccoyo Ore, F.; López, F.d.L.M.; Valderrama Negrón, A.C.; Ludeña Huaman, M.A. Fe_3O_4/Poly (acrylic acid) Composite Hydrogel for the Removal of Methylene Blue and Crystal Violet from Aqueous Media. *Chemistry* **2025**, *7*, 156. [CrossRef]
89. Brar, S.K.K.; Soni, G.K.; Bharti, A.; Wangoo, N.W.; Sharma, R.K. Self-assembled fibrils based on novel N-aryl pseudo-peptoids for effective adsorption of cationic dyes from wastewater. *Mater. Sci. Eng. B* **2025**, *318*, 118248. [CrossRef]
90. Okoh, E.I.; Immanuel, O.M. Assessment of Biodegradation and Phytotoxicity of Azo Dyes Methyl Orange and Crystal Violet by Escherichia Coli and Bacillus Subtilis. *South Asian J. Res. Microbiol.* **2024**, *18*, 1–8. [CrossRef]
91. Bharagava, R.N.; Mani, S.; Mulla, S.I.; Saratale, G.D. Degradation and decolourization potential of an ligninolytic enzyme producing Aeromonas hydrophila for crystal violet dye and its phytotoxicity evaluation. *Ecotoxicol. Environ. Saf.* **2018**, *156*, 166–175. [CrossRef]

Disclaimer/Publisher's Note: The statements, opinions and data contained in all publications are solely those of the individual author(s) and contributor(s) and not of MDPI and/or the editor(s). MDPI and/or the editor(s) disclaim responsibility for any injury to people or property resulting from any ideas, methods, instructions or products referred to in the content.